ELSEVIER

Advances in Water Resources 23 (2000) 517–530

Advances in Water Resources

FLOTRAN, a three-dimensional ground water model, with comparisons to analytical solutions and other models ☆

Anthony W. Holder [a,*], Philip B. Bedient [a,1], Clint N. Dawson [b,2]

[a] Department of Environmental Science and Engineering, Rice University, 6100 Main Street, Houston, TX 77005-1892, USA
[b] Texas Institute for Computational and Applied Mathematics, University of Texas, Austin, TX 78712, USA

Received 8 September 1998; received in revised form 25 August 1999; accepted 26 August 1999

Abstract

FLOTRAN is a ground water flow and transport model developed in the past few years which takes advantage of recent advances in numerical methodology. FLOTRAN solves the governing equations for flow and contaminant transport using Godunov-mixed methods, in which a higher-order Godunov method is used to approximate the advective flux, and a mixed finite element method is used for the dispersive transport. A mixed finite element method is also used to solve the flow equation. As part of the development of this new model, we have tested it against known analytical and numerical solutions to the equations approximated by the model. In this work, we have tested FLOTRAN against 1-D and 2-D analytical solutions, Galya's 3-D horizontal plane source solution, two radial semi-analytical solutions, and two numerical models, BIOPLUME II and MT3D. We have also tested FLOTRAN on a hypothetical partially saturated flow problem. FLOTRAN performed well on these tests, generally matching analytical solutions to within a few percent, and matching as well as or better than the other numerical models in most cases.

Keywords: Numerical models; 3-D models; Ground water; Hydrodynamics; Pollutants; Transport

1. Introduction

Recent advances in numerical methodology have led to the development of a 3-D ground water flow and contaminant transport model called FLOTRAN. The numerical methods used in FLOTRAN [5,6,8] provide excellent mass balance characteristics, fast solution times, and flexibility in choosing modeling conditions, such as grid definition (uniform and variable grid spacing), boundary conditions (constant head or constant flux for flow, inflow and outflow/no-flow for transport), and wells (injection, extraction, and monitoring wells). In addition, FLOTRAN incorporates linear sorption, biodegradation (via Monod or fast equilibrium kinetics), and first-order decay into its solution of the ground water contaminant transport equations, and can model multiple components, allowing the user to simulate several contaminants in one model run.

FLOTRAN uses a mixed finite element method for flow on structured rectangular grids. This method conserves mass elementwise (for steady flow) and provides second-order accurate velocities at the edges of the rectangular elements [24]. By comparison, the well-known FEMWATER [28] and MODFLOW [17] flow models are based on a standard piecewise linear Galerkin finite element approximation for head. This approach is not elementwise conservative, and velocities are at best first-order accurate.

For transport, FLOTRAN uses a higher-order Godunov method for advection combined with a mixed finite element method for diffusion. This method is also based on elementwise conservation, and captures sharp fronts stably with a modest amount of numerical diffusion. In contrast, the well-known model BIOPLUME II [19], uses a method of characteristics, in particular the USGS method of characteristics (MOC) model [16]. While its popularity indicates the confidence that

☆ A version of the FLOTRAN code is available to researchers at non-profit institutions by sending a request to the third author.

* Corresponding author. Fax: +1-713-282-5239.
E-mail addresses: anthony@rice.edu (A.W. Holder), bedient@rice.edu (P.B. Bedient), clint@ticam.utexas.edu (C.N. Dawson).
[1] Fax: +713-285-5239.
[2] Fax: +512-471-8694.

0309-1708/00/$ - see front matter
PII: S0309-1708(99)00040-8

BIOPLUME II has among environmental professionals, it is susceptible to mass balance errors, and is limited by its two-dimensionality.

MT3D and RT3D [4,29]) are also popular transport codes and are based on particle tracking, which advects mass contained in particles through the flow field. Particle tracking codes generally model advective transport well, however the way in which dispersion is incorporated is computationally expensive, since dispersion is modeled explicitly, and gives rise to mass balance errors, since concentrations must be averaged onto a grid. Wells and variable thickness aquifers can also cause mass balance errors in particle tracking codes.

BIOPLUME II, MODFLOW, and MT3D have been used widely for modeling contamination extent, and for evaluating remediation options. These codes, while still useful, have some drawbacks. Numerical methodology has advanced since they were written. Presented herein is a new numerical ground water flow and contaminant transport model, which is robust, stable, and computationally efficient. The purpose of this paper is to describe FLOTRAN, and to present some of the testing the transport portion of the code has undergone. We also present one case involving unsaturated flow and transport. In Section 2, we outline the numerical methods used in FLOTRAN. In Section 3, we discuss our approach for testing the model, and in Section 4, we present results for several tests. Finally, we end with some conclusions and plans for future work.

2. Description of FLOTRAN

FLOTRAN solves Richard's equation for flow in unsaturated conditions, which reduces to the standard flow equation for confined/saturated conditions, combined with a system of advection–diffusion-reaction equations describing contaminant transport. It assumes a 3-D, logically rectangular domain, but allows for fairly general geometries by using smooth mappings between the logically rectangular domain and a rectangular computational domain. Therefore, the algorithms used in the method are described in the context of brick-shaped elements.

FLOTRAN solves the governing flow equation using the mixed finite element method for spatial discretization and fully implicit time discretization. The flow equation is of the form

$$\frac{\partial\theta(\Psi)}{\partial t}+S_{\mathrm{s}}\frac{\partial h}{\partial t}+\nabla\cdot\mathbf{v}=q, \tag{1}$$

where $\mathbf{v}$ is the Darcy velocity, q represents sources and sinks, S_{s} the specific storage, θ the moisture content, h the hydraulic head, and $\Psi=h-z$ is the pressure head. The mixed finite element method applied to flow equations has been described in numerous papers; the version employed to solve (1) is defined in the context of linear elliptic equations in [1]. In this method, hydraulic head and Darcy velocity are simultaneously approximated, with hydraulic head approximated by a constant in each element. Numerical integration is used to reduce the finite element equations to a cell-centered finite difference scheme in head variables only. Here we outline the method for Richard's equation

Consider an element $B_{ijk}\in\Re^3$ with $B_{ijk}=[x_{i-1/2},x_{i+1/2}]\times[y_{j-1/2},y_{j+1/2}]\times[z_{k-1/2},z_{k+1/2}]$.

Let (x_i, y_j, z_k) denote the midpoint of B_{ijk}.

In the mixed finite element method of lowest order, one approximates h and ψ by constants h_{ijk} and ψ_{ijk} on B_{ijk}, and $v=(v^x,v^y,v^z)$ is approximated at the centers of the faces. Integrating (1) over B_{ijk} and in time from t^n to t^{n+1} and applying the divergence theorem we have

$$\frac{\theta\left(\psi_{ijk}^{n+1}\right)-\theta(\psi_{ijk}^{n})}{t^{n+1}-t^{n}}+(S_{\mathrm{s}})_{ijk}\frac{h_{ijk}^{n+1}-h_{ijk}^{n}}{t^{n+1}-t^{n}}+\frac{v_{i+1/2,j,k}^{x,n+1}-v_{i-1/2,j,k}^{x,n+1}}{x_{i+1/2}-x_{i-1/2}}+\frac{v_{i,j+1/2,k}^{y,n+1}-v_{i,j-1/2,k}^{y,n+1}}{y_{j+1/2}-y_{j-1/2}}+\frac{v_{i,j,k+1/2}^{z,N+1}-v_{i,j,k-1/2}^{z,N+1}}{z_{k+1/2}-z_{k-1/2}}=q_{ijk}^{n+1}. \tag{2}$$

By Darcy's law $v=-K(\psi)\nabla h$. When mapping from a logically rectangular domain to a rectangular computational domain, it is possible to obtain a coefficient K, which is a full tensor. Therefore,

$$K=\begin{bmatrix}K^{xx}&K^{xy}&K^{xz}\\K^{xy}&K^{yy}&K^{yz}\\K^{xz}&K^{yz}&K^{zz}\end{bmatrix}.$$

Define $\tilde{v}_{i+1/2,j,k}^{x}=(h_{i+1,j,k}-h_{i,j,k})/(x_{i+1}-x_i)$, with similar definitions for $\tilde{v}_{i,j+1/2,k}^{y}$ and $\tilde{v}_{i,j,k+1/2}^{z}$.

Then define

$$v_{i+1/2,j,k}^{x}=K_{i+1/2,j,k}^{xx}\tilde{v}_{i+1/2,j,k}^{x}+\frac{1}{4}\sum_{\ell=0}^{1}\sum_{m=0}^{1}(K^{xy}\tilde{v}^{y})_{i+\ell,j+1/2-m,k}+\frac{1}{4}\sum_{\ell=0}^{1}\sum_{m=0}^{1}(K^{xz}\tilde{v}^{z})_{i+\ell,j,k+1/2-m}.$$

Substituting $\tilde{v}$ into this equation, and substituting into (2), we obtain a non-linear system of equations in $h_{i,j,k}^{n+1}$.

These equations are solved using a damped Newton method with linesearch backtracking to aid convergence from poor starting guesses [9]. The Jacobian equations which arise at each Newton step are solved using a preconditioned orthomin iterative procedure.

Flux boundary conditions $v\cdot n=g$ are handled by setting the appropriate velocity $v^x, v^y, v^z=g$, depending on which face the condition is prescribed. Dirichlet boundary conditions $h=h_{\mathrm{D}}$ are specified through the definition of $\tilde{v}$. Thus these conditions are specified weakly.

For the case of saturated flow, $\theta = \theta_s$, it was shown in [1] that v and h are approximated to second order accuracy at the face centers and cell centers, respectively. Recently, in [27], the mixed method applied to Richard's equation was analyzed. Here the precise rate of convergence is not known a priori because the smoothness of solutions is not known.

The Darcy velocities and moisture content computed from the flow are used in the system of transport equations for each contaminant species. These equations model the advection, diffusion, and chemical reactions of species in the system. Each equation is of the form

$$\frac{\partial \theta c}{\partial t} + \nabla \cdot (\mathbf{v}c - D\nabla c) = q\hat{c} + g, \tag{3}$$

where c is the contaminant concentration, D the diffusion/dispersion tensor, and g incorporates chemical reactions; g may be a function of several species in the system. At sources $\hat{c}$ is specified. At sinks $\hat{c} = c$.

Eq. (3) is solved numerically using a time-splitting approach. Given an approximation $C(t)$ to $c(t)$ at some time t, the approximation advances to time $t + \delta t$ by advecting and diffusing $C(t)$, which gives an intermediate solution $\bar{C}(t + \delta t)$, then incorporating reactions using $\bar{C}(t + \delta t)$ as initial conditions. This ultimately gives $C(t + \delta t) \approx c(t + \delta t)$. This type of splitting has been analyzed in [25], and has been adopted and modified by a number of other researchers [21]. The advantages of this approach are that the advection and diffusion of each component can be performed separately (and in parallel if desired), advection–diffusion and reactions can be modeled using appropriately sized time steps, and different reaction models can be easily incorporated.

Advection and diffusion/dispersion are modeled using the Godunov-Mixed Method, outlined and analyzed by Dawson [6,7]. In the version of this scheme used in FLOTRAN, a second-order accurate Godunov procedure is used to approximate the advective flux, and a mixed finite element method, similar to that used for the flow equation, is used to incorporate diffusion/dispersion. The resulting scheme is a cell-centered finite difference method for contaminant concentrations. The advective flux is incorporated explicitly in time, while the diffusion/dispersion step is implicit. By modeling advection explicitly and diffusion implicitly, a symmetric, diagonally dominant and positive definite system of equations at each time-step is obtained. This system is easily solved using Jacobi preconditioned conjugate gradient. Although contaminant concentrations are only approximated by constants in each cell, the Godunov-Mixed Method is second order accurate in space and first-order accurate in time at the center of each element. This has been observed both theoretically and computationally.

Let C_{ijk} be the approximation to c on B_{ijk}, and let $F = (F^x, F^y, F^z) \approx -D\nabla c$. Integrating (3) over B_{ijk} and from t^n to t^{n+1},

$$\begin{aligned}&\frac{\theta^{n+1}_{ijk} C^{n+1}_{ijk} - \theta^n_{ijk} C^n_{ijk}}{t^{n+1} - t^n} + \frac{v^{x,n+1}_{i+1/2,j,k} C^{n+1/2}_{i+1/2,j,k} - v^{x,n+1}_{i-1/2,j,k} C^{n+1/2}_{i-1/2,j,k}}{x_{i+1/2} - x_{i-1/2}} \\ &\quad + \frac{F^{x,n+1}_{i+1/2,j,k} + F^{x,n+1}_{i-1/2,j,k}}{x_{i+1/2} - x_{i-1/2}} \\ &\quad + \text{similar terms in } y \text{ and } z = q^{n+1}_{ijk} \hat{C}^{n+1}_{ijk},\end{aligned}$$

where $\hat{C}$ is specified if $q > 0$ and $\hat{C} = C$ if $q < 0$.

A variant of the higher-order Godunov method described in [2] is used to calculate the flux term $C^{n+1/2}_{i+1/2,j,k}$. Ignoring diffusion (which is usually small relative to advection), consider the advection equation

$$\frac{\partial(\theta c)}{\partial t} + \nabla \cdot (vc) = 0$$

or

$$\frac{\partial c}{\partial t}\theta + \frac{\partial \theta}{\partial t} c + v^x \frac{\partial c}{\partial x} + c\frac{\partial v^x}{\partial x} + \frac{\partial (v^y c)}{\partial y} + \frac{\partial (v^z c)}{\partial z} = 0.$$

By Taylor series

$$\begin{aligned}c^{n+1/2}_{i+1/2,j,k} &\approx c^n_{ijk} + \frac{\Delta t}{2}\frac{\partial c}{\partial t} + \frac{\Delta x}{2}\frac{\partial c}{\partial x} \\ &= c^n_{ijk} - \frac{\Delta t}{2}\frac{1}{\theta}\left[\frac{\partial \theta}{\partial t} c + v^x \frac{\partial c}{\partial x}\right. \\ &\quad \left. + c\frac{\partial v^x}{\partial x} + \frac{\partial (v^y c)}{\partial y} + \frac{\partial (v^z c)}{\partial z}\right] + \frac{\Delta x}{2}\frac{\partial c}{\partial x},\end{aligned} \tag{4}$$

where the last two terms are approximated at (x_i, y_j, z_k) and t^n.

The term $(\partial c/\partial x)_{ijk}$ is approximated using a "slope-limiting" procedure. If C^n_{ijk} is a local maximum or minimum (compared to all cells which share an edge or vertex with B_{ijk}) then we simply set $C^{n+1/2}_{i+1/2,j,k} = C^n_{ijk}$. Otherwise we compute

$$\min\left(\frac{|C_{i+1,j,k} - C_{i,j,k}|}{x_{i+1} - x_i}, \frac{|C_{i,j,k} - C_{i-1,j,k}|}{x_i - x_{i-1}}\right)$$

and approximate $(\partial c/\partial x)_{ijk}$ by the minimum multiplied by the appropriate sign. Let $\partial_x C^n_{ijk}$ denote this approximation.

The transverse flux terms $v^y c$ and $v^z c$ in (4) are computed by first-order upwinding.

Let

$$\tilde{c}_{i,j+1/2,k} = \begin{cases} c_{i,j,k}, & v^y_{i,j+1/2,k} > 0, \\ c_{i,j+1,k}, & v^y_{i,j-1/2,k} < 0. \end{cases}$$

Then

$$C^{n+1/2}_{i+1/2,j,k} = C^n_{ijk} - \frac{\Delta t}{2}\frac{1}{\theta^n_{ijk}}\left[\frac{\theta^{n+1}_{ijk}-\theta^n_{ijk}}{t^{n+1}-t^n}C^n_{ijk} + v^{x,n}_{ijk}\partial_x C^n_{ijk} + C^n_{ijk}\left(\frac{v^{x,n}_{i+1/2,j,k}-v^{x,n}_{i-1/2,j,k}}{x_{i+1/2}-x_{i-1/2}}\right) + \left(\frac{(v^y\tilde{c})^n_{i,j+1/2,k}-(v^y\tilde{c})^n_{i,j-1/2,k}}{y_{j+1/2}-y_{j-1/2}}\right) + \left(\frac{(v^z\tilde{c})^n_{i,j,k+1/2}-(v^z\tilde{c})^n_{i,j,k-1/2}}{z_{k+1/2}-z_{k-1/2}}\right)\right] + \frac{\Delta x}{2}\partial_x C^n_{ijk}.$$

The diffusive flux $F^x_{i+1/2,j,k}$ is defined similarly to $v^x_{i+1/2,j,k}$ with K replaced by D and h replaced by C.

FLOTRAN handles inflow and outflow/no-flow boundary conditions for transport. At an inflow boundary ($v\cdot n<0$) we assume $(vc - D\nabla c)\cdot n = vc_I\cdot n$, where c_I is specified. FLOTRAN enforces this condition (for example, at an x boundary face) by setting

$$v^{x,n}_{i+1/2,j,k}C^{n+1/2}_{i+1/2,j,k} + F^{x,n+1}_{i+1/2,j,k} = v^{x,n}_{i+1/2,j,k}c_I.$$

At outflow/no-flow boundaries (where $v\cdot n \geqslant 0$), we assume $(D\nabla c)\cdot n = 0$. This is easily enforced through the flux approximation F.

3. Model testing

Testing ground water models assures that the models may be relied upon to closely approximate the ground water flow and transport equations. However, literature on model testing methodologies is sparse. Huyakorn et al. [15] designed and implemented several tests for numerical models. He then demonstrated the use of these tests on SEFTRAN, a 2-D model which uses finite-element approximations to the flow and transport equations. This testing methodology uses a three-level approach: analytical solutions, heterogeneous/anisotropic tests, and field validation tests. In his report, Huyakorn presents the model scenario, the analytical form of the solution, and tabulated analytical solutions for the specific test case. These tests form the basis of the International Ground Water Modeling Center's recommendations for model testing [22]. Aside from the Huyakorn report, most model testing information in the literature is limited to specific tests applied to specific models for narrow purposes (e.g., [10,23]).

The testing performed on FLOTRAN [13] includes four tests against 1-, 2-, and 3-D analytical solutions, two tests against semi-analytical solutions with radial flow fields, a comparison with results from the BIOPLUME II code on a hypothetical site, and a test involving flow and transport in a partially saturated region.

The four analytical tests include (A.1) a 1-D constant concentration simulation, two tests with a uniform 2-D flow field, (A.2) a constant injection of contaminant, and (A.3) a slug of contaminant, and (A.4) 3-D flow of contaminant from a horizontal plane source (including a comparison to MT3D and the horizontal plane source solution for the same scenario). The two semi-analytical tests with radial flow fields are (B.1) injection/recovery from a single injection well, and (B.2) injection/recovery from two different wells.

Huyakorn relied upon visual comparisons for determining whether the model matched the analytical solution. In order to give a quantitative measure of how FLOTRAN matches the analytical solutions, we computed various error measures to quantify the difference between the analytical solution and the model.

4. Description of testing

4.1. Tests with analytical solutions

The first four analytical tests are based on methods developed to test SEFTRAN [15]. These tests are all based on well known solutions to the advection–dispersion equation in simple situations. The last test is based on the 3-D horizontal plane source solution [11]. Table 1 shows the major grid and variable choices for the first four analytical solution tests.

4.1.1. Test A.1: 1-D continuous source

Test A.1 is a simulation of 1-D transport in a semi-infinite column with a constant concentration boundary condition. Flow is assumed to be unidirectional and contaminant is assumed to be introduced as a constant concentration (C_0) along the entire upgradient boundary. The analytical solution [18] is

$$\frac{C}{C_0} = 0.5\left\{\operatorname{erfc}\left(\frac{x-vt}{2\sqrt{Dt}}\right) + \exp\left(\frac{vx}{D}\right)\operatorname{erfc}\left(\frac{x+vt}{2\sqrt{Dt}}\right)\right\}, \tag{5}$$

where v is the interstitial velocity of the ground water, α is the dispersivity, and $D = \alpha v$ is the dispersion coefficient.

Four subcases were simulated, and are characterized by the cell Peclet number ($Pe = \Delta x/\alpha$), as given in Table 2. Computed values of C/C_0 are plotted in Fig. 1 at elapsed times of 25 and 50 days and are compared to the analytical solutions using Eq. (5). The 'average absolute errors' for each case are also shown in Table 2 for the simulation results at 25 and 50 days. The average absolute error over a region is given by

$$\frac{1}{(i_2-i_{1+1})(j_2-j_{1+1})(k_2-k_{1+1})}\sum_{i=i_1}^{i_2}\sum_{j=j_1}^{j_2}\sum_{k=k_1}^{k_2}\frac{|C_{ijk}-c_{ijk}|}{C_0}. \tag{6}$$

Table 1
Major grid and aquifer parameters for Tests A.1–A.4

Simulation parameter	Problem A.1 1-D constant concentration source	Problem A.2 2-D constant point source (Fine, Med., Coarse)	Problem A.3 2-D slug point source	Problem A.4 horizontal plane source (HPS)
N_x	40	39, 39, 13	49	32
N_y	2	20, 10, 5	11	21
N_z	2	2	2	15
Δx (m)	5	60, 60, 180	Variable	Variable
Δy (m)	10	15, 30, 60	5	5
Porosity, θ	0.25	0.35	0.35	0.38
Δz (m)	10	33.5	5	2
Conductivity, K_x (cm/s)	0.01157	0.0186	0.1	0.005
Conductivity, K_y (cm/s)	0.01157	0.0186	0.1	0.005
Dispersivity, α_L (m)	5.0, 2.0, 0.2, 0.0	21.3	4	5
Dispersivity, α_T (m)	–	4.3	1	0.5
Gradient, $\partial h/\partial l$	0.01	0.01	0.0231	0.0096
Injection rate, Q (m^3/s)	N/A	0.0983	N/A	0.8 (m/yr) infiltration
Initial Conc., C_0 (mg/l)	1.0	5000	0.4	100.0

Table 2
Test A.1, subcases and results

Peclet number (non-dimensional)	Dispersivity (m)	Average absolute errors (% of C_0)	
		25 days	50 days
2	5	0.32	0.22
5	2	0.32	0.16
50	0.2	0.92	0.42
∞	0.0	0.0	0.0

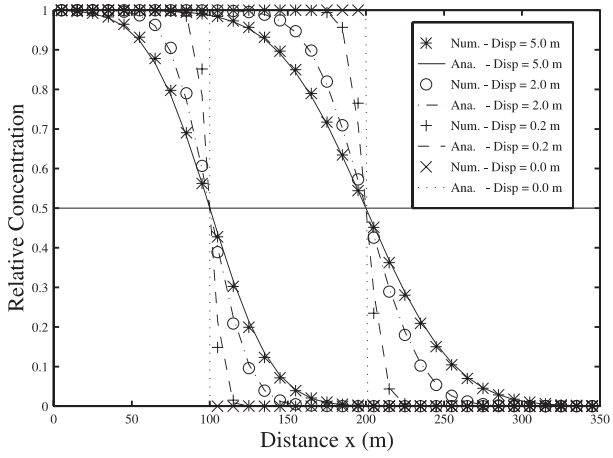

Fig. 1. Test A.1, one-dimensional continuous source – FLOTRAN vs. analytical solution. Results are shown for $t = 25$ days and $t = 50$ days.

In this case, since the problem is 1-D $i_1 = 1$, $i_2 = N_x$, $j_1 = j_2 = k_1 = k_2 = 1$. Thus (6) is equivalent to the L_1 norm of the error, scaled by the length of the domain and the injected concentration.

4.1.2. Test A.2: uniform 2-D flow, continuous injection

Test A.2 involves continuous injection of contaminant into a well located in an otherwise uniform 2-D aquifer. The solution for this problem assumes that the contaminant is introduced as a mass flux at a point source [26]. The model will simulate these conditions by assigning a low flow rate and high concentration at the well located at the point source, thus keeping the radial flow to a minimum.

Three grids were used in this simulation, so that the sensitivity to mesh size could be determined. The grid choices are labeled coarse, medium, and fine. All grid and simulation parameters are given in Table 1, while Table 3 shows the cell Peclet numbers and average absolute errors. Dimensionless variables used in the plots are calculated according to the following formulas: dimensionless distance along the x-axis, $x_D = x/(2\alpha_L)$; along the y-axis, $y_D = y/(2\alpha_L)$; and dimensionless concentration $C_D = 2\pi\sqrt{\alpha_L\alpha_T}(vC/QC_0)$, where v is the background seepage velocity, Q is the injection rate, α_L and α_T are the longitudinal and transverse dispersivities, respectively, and C and C_0 are the 'present' and initial concentrations, respectively.

Results of the simulation are shown in Figs. 2–4 for the coarse, medium, and fine meshes, respectively. Snapshots of concentrations are taken at times of 500, 1000, 2000, and 2800 days. The analytical solution is

Table 3
Test A.2, subcases and results

Grid size	X Peclet number (non-dimensional)	Y Peclet number (non-dimensional)	Average absolute errors (% of C_0)
Coarse	8.4	14.0	8.0
Medium	2.8	7.0	2.5
Fine	2.8	3.5	0.5

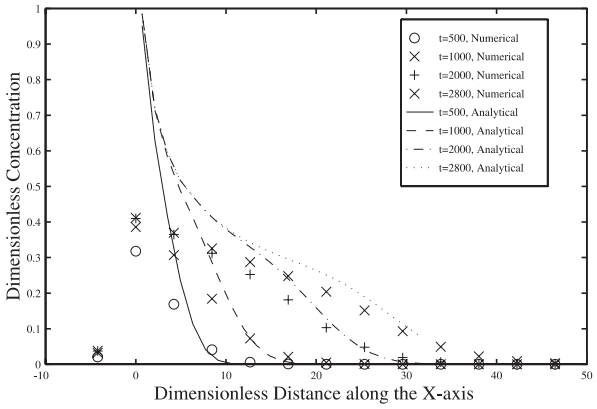

Fig. 2. Test A.2, point source in two-dimensional uniform flow field – FLOTRAN vs. analytical solution. Coarse mesh.

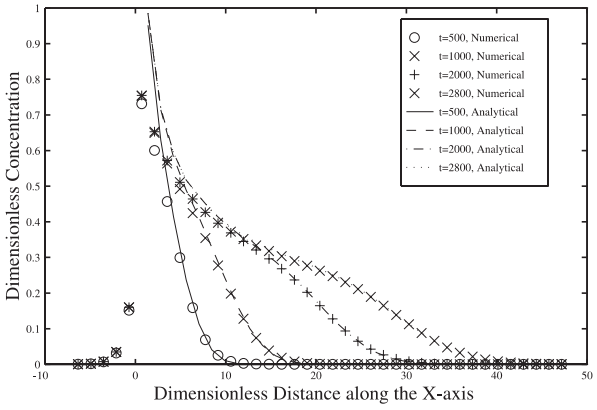

Fig. 3. Test A.2, point source in two-dimensional uniform flow field – FLOTRAN vs. analytical solution. Medium mesh.

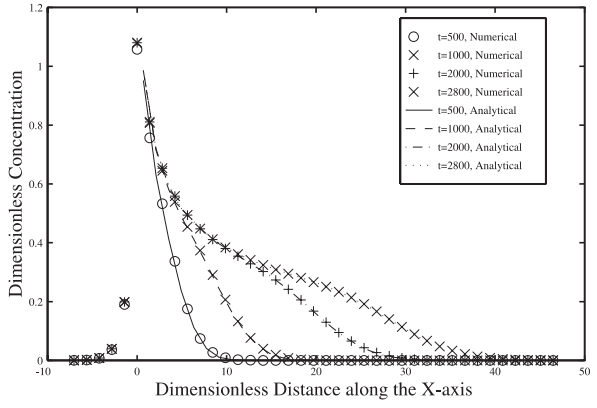

Fig. 4. Test A.2, point source in two-dimensional uniform flow field – FLOTRAN vs. analytical solution. Fine mesh.

plotted for comparison. The analytical solution for this test is tabulated in [15]. As expected, the fine mesh shows the best agreement between analytical and numerical solutions. The error reported in Table 3 is the average absolute error along the centerline of the plume, averaged over all four times. That is, the error was computed using (6), summing over elements in the center of the plume. As seen in the table, decreasing the grid size, and therefore, the Peclet number, increases the accuracy of this simulation significantly.

FLOTRAN computes the concentration in the cells as an average over the total mass in the cell divided by the volume of the cell, so in a situation like this, large cells affect the concentration by averaging in what should be clean water with the contaminated water. Using this computational method allows FLOTRAN to maintain cell by cell mass balance, but may affect the concentrations near a source due to the averaging of clean water with contaminated water in a single cell. This effect may be observed in Fig. 2 (coarse mesh). Near the source, the numerical concentration for the coarse mesh is less than one half the analytical concentration. Moreover, the solution is smeared upstream due to the fact that the source was treated as an injection well. Farther away and a later times, however, the concentrations approach the analytical solution concentrations. Both the medium and fine meshes give better performance, with the fine mesh matching the analytical solution very well, both visually, and using the average absolute error.

The analytical solution assumes a point source, with no disturbance of the flow field. In order to capture this effect numerically with an injection well, the grid cells need to be small enough so that the injection rate in the well's grid cell causes the entire cell to be mostly contaminated after the first time step. Thus, the cell Peclet number should be as low as possible, in both the longitudinal and transverse directions. From this series of tests, it appears that a cell Peclet number of 3 or lower is sufficient.

The mass conservation properties of FLOTRAN are well demonstrated by this example. For the 'coarse' grid case described above, mass balance information was analyzed. A mass balance was manually calculated by summing the total mass in the model domain after each time step, and comparing to the expected mass injected at the well. After the first time step (100 days), the mass balance error was $2 \times 10^{-6}\%$, and after ten time steps (1000 days), the mass balance error was $5 \times 10^{-6}\%$.

4.1.3. Test A.3: uniform 2-D flow, slug of contaminant

Test A.3, like Test A.2, tests advection and dispersion in a uniform flow field, however the source of contamination is changed to a slug of contaminant, instead of a continuing source. This accomplishes two goals: (1) it tests the ability of FLOTRAN to trace a slug as it flows downgradient, and as it disperses in two dimensions, and (2) it tests its ability to simulate a case in which the longitudinal and transverse dispersivities are different [15].

Sauty's solution [20] is tabulated in [15]. In this scenario, the contaminant is introduced into the system at $x = y = 0$ and allowed to flow downstream. This simulation is symmetrical about the x-axis and can be run on half of the domain, simulating only the $+y$ direction. The grid is variable, with smaller cells ($\Delta x = 5$ m) near the release point, and larger cells ($\Delta x = 10$ m) downstream. The remaining parameters are given in Table 1. The cell Peclet numbers for this test are 1.25 near the source in the longitudinal direction, 2.5 downstream from the release point in the longitudinal direction, and 5 in the transverse direction. The Peclet numbers near the release point are both close to the value of 3 recommended earlier, with the average Peclet number being almost exactly 3.

The analytical solution is compared to the numerical solution given by FLOTRAN in Fig. 5. At t =3.96 days, the numerical solution differs slightly from the analytical solution, especially at the center of mass of the solute plume. At the two later times, there is very good agreement between the analytical and numerical solutions. This behavior is expected, since the analytical solution assumes a point source, and the numerical solution requires a finite (25 m^2) source. In such a case, one would expect the solutions to agree better at later time steps. The errors calculated for this simulation are the average absolute errors along the centerline of the plume divided by the maximum concentration at a given time. For $t = 3.96$, 10.59 and 16.59 days, the calculated errors are 0.86%, 0.68% and 0.48%, respectively.

4.1.4. Test A.4: HPS solution

The Horizontal Plane Source solution solves for the concentration in a 3-D aquifer of either finite or infinite vertical extent due to infiltration of contaminated water through a horizontal plane at the water table [11]. The HPS code calculates the concentration at one point in space and time, and was modified to loop over space and time to give results for the complete 3-D aquifer at all time steps. For this comparison, eight observation points were selected, near the source, far from the source, along the centerline of the plume, and near the edge of the 'landfill', near the water table, and away from the water table. Fig. 6 depicts a conceptual model for the simulation, including locations of the landfill and observation points. The grid setup and other simulation parameters are given in Table 1. A non-uniform grid was selected for the FLOTRAN simulation. The scenario was also set up in MT3D for comparison.

Fig. 7 shows the vertical concentration profiles along the centerline of the plumes for HPS, FLOTRAN, and MT3D. The contamination extends downstream from the landfill and is symmetric perpendicular to the direction of flow. The concentration is highest near the source, and the contaminant stays near the water table, with the 1.0 mg/l contour extending about 15 m down. The three models produced very similar results, as can

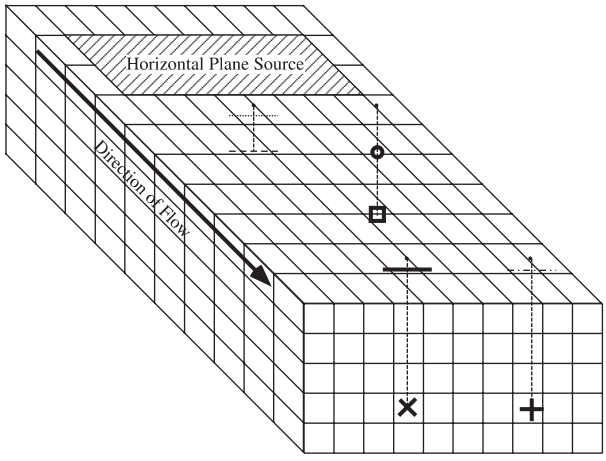

Fig. 6. Test A.4, conceptual model of configuration for horizontal plane source simulation. The observation points are vertically below the points along the top plane, with two elevations for each horizontal point.

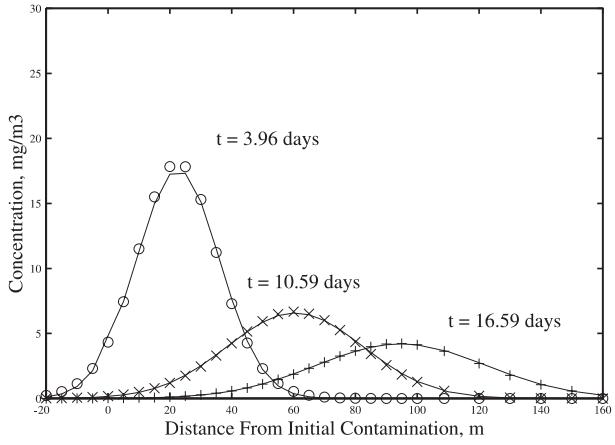

Fig. 5. Test A.3, slug of contaminant in uniform two-dimensional aquifer–FLOTRAN vs. analytical solution.

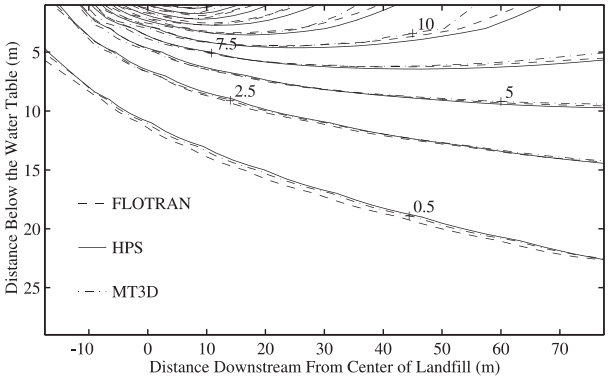

Fig. 7. Test A.4, HPS, FLOTRAN, and MT3D solutions along the centerline of the plume.

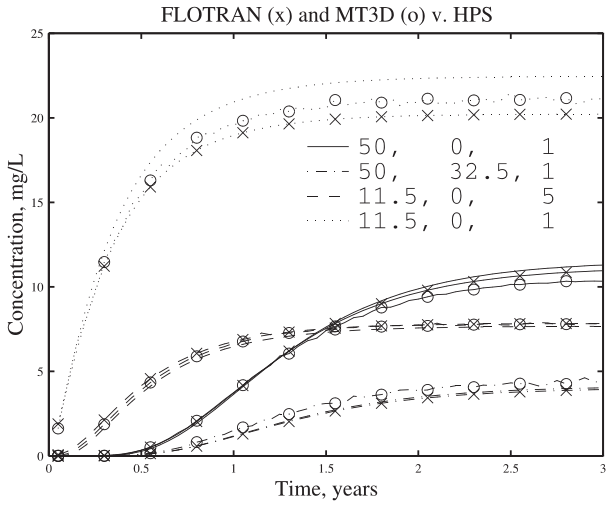

Fig. 8. Test A.4, HPS (no symbol) vs. FLOTRAN (×) and MT3D (○) at 4 points in space. The linetypes correspond to the locations shown in Fig. 6.

be seen in the figure. The largest differences are very near the source, where FLOTRAN and MT3D both predict higher concentrations than HPS; away from the source, the contours for all three are very close. Galya [11] notes that a multi-point source model tends to predict higher concentrations near the source than the HPS model, which assumes that the source is spread evenly over the entire source. In his comparisons, the closest point is located 20 m from the origin, or 14 m from the edge of the landfill. In this simulation, the closest point is 11.5 m from the origin, and 1.5 m from the edge of the landfill. A small overprediction at that point is unavoidable.

In this simulation, FLOTRAN was dramatically faster than either MT3D or HPS on a Sun Sparc 20 (100 MHz). For identical systems, using $21 \times 32 \times 15$ grids, and a 5 yr time span, MT3D and HPS took between 1.5 and 3 h to complete the simulation, where FLOTRAN ran the simulation in about 10 min. The difference in run times for the numerical codes (FLOTRAN and MT3D) was largely due to the difference in time step size. The time step FLOTRAN chose was larger because of the implicit treatment of dispersion in the code. Treating dispersion implicitly requires more computational effort for each time step, but allows selection of larger time steps by the code. Smaller time steps are required in explicit codes such as MT3D to avoid numerical instability. HPS is limited by the fact that for each time T^n, the code must perform the numerical integration from $t = 0$ to $t = T^n$ instead of $t = T^{n-1}$ to $t = T^n$. The code for HPS was not designed to perform 3-D multi-time-step calculations, and the modifications made by the authors to allow these calculations are undoubtedly inefficient.

Fig. 8 shows the concentration at four points as a function of time. Three curves are presented for each observation point, one for each model. The line types shown in Fig. 8 correspond to the observation point symbols in Fig. 6, with one line type for each observation point. HPS is represented by a clean line, FLOTRAN by a line with × marks on it, and MT3D by a line with ○ marks on it. In Table 4, we have computed the absolute error at each of the eight observation points, averaged over time.

In general, the FLOTRAN solution is lower near the source, and slightly higher far from the source than the semi-analytical HPS solution. This behavior is consistent with the presence of numerical dispersion, present in all numerical models to some extent, which reduces peak concentrations in accordance with the 'total' dispersion, which is equal to the modeled dispersion plus the numerical dispersion.

4.2. Tests with semi-analytical solutions for radial flow fields

The next two tests were performed to compare against testing performed on the MOC code which is the basis for BIOPLUME II [10]. In his paper, El-Kadi voiced a concern that MOC was being used to model scenarios which were too stressful for the code. In particular, he simulated two cases with radial flow around one or two wells, with very large (900×900 ft^2) cells, small grids (9×9), and relatively high pumping rates. FLOTRAN has been tested in the same situations,

Table 4
Average absolute errors for the HPS vs. FLOTRAN Test

Symbol on Fig. 6	Distance from center of landfill (m)			FLOTRAN run avg abs diff (mg/l)	MT3D test avg abs diff (mg/l)
	x	y	z		
–	50	0	1	0.231	0.607
–·–·–	50	32.5	1	0.080	0.335
×	50	0	15	0.066	0.028
+	50	32.5	5	0.023	0.041
– – –	11.5	0	5	0.219	0.173
○	11.5	32.5	5	0.107	0.228
·····	11.5	0	1	2.012	1.243
□	11.5	32.5	15	0.019	0.010

because it is almost certain that eventually it will also be used in such stressful situations, and the user should be aware of any problems which may arise from such use.

4.2.1. Test B.1: radial flow: injection and subsequent extraction from the same well

In this situation, contaminated water is injected into a 9×9 aquifer for a time t_1, then the flow is reversed, and water is removed from the aquifer. An analytical expression has been derived to approximate the concentration in the well during this process [12]. The expression reads

$$\frac{C}{C_0} = \frac{1}{2}\operatorname{erfc}\left\{ -V \Big/ \left[\frac{16}{3}\frac{\alpha}{R}(2 - V|V|^{1/2}) \right]^{1/2} \right\}, \tag{7}$$

where

$$V = (2t_1 - t)/t_1 \tag{8}$$

and

$$R = (Qt_1/\pi\theta B)^{1/2}. \tag{9}$$

In Eqs. (7)–(9), t is the time since the beginning of the injection cycle and t_1 is the time at which injection stops and recovery begins. Therefore, V is not a physical volume, but is a measure of how much of the injected water remains in the subsurface at time t. When $V = 0$, $(t = 2t_1)$, the same amount of water has been removed from the well in the recovery stage as was injected into the well in the injection stage. Other variables are: Q, the flow rate (assumed to be the same in injection and recovery), θ, the porosity, and B, the (constant) thickness of the aquifer.

Four subcases were simulated in this test case. The subcases test different dispersivities, injection times, and flow rates. These parameters are given in Table 5, while the parameters which are common to all of the subcases are defined in Table 6. The four subcases were also simulated with BIOPLUME II, recreating the work of El-Kadi.

Fig. 9a and b illustrate the results of the experiments B.1.a and B.1.b for the FLOTRAN and BIOPLUME II (MOC) simulations. The other subcases had similar results, and are not shown. This figure consists of three curves each, FLOTRAN, BIOPLUME II, and the Gelhar and Collins solution for the test dispersivity, and for a second dispersivity, to be discussed below.

The closeness of fit between the analytical solution and the numerical solution are measured in this case by computing the absolute error at the injection/extraction well at each time, and averaging over time. The errors are given in Table 7 as a percent of the injection concentration. In spite of the severe stresses in this simulation, the results are consistently within 10 to 15% of the value given by the analytical solution.

Table 5
Variable parameters for subcases B.1.a, B.1.b, B.1.c, and B.1.d.

Subcase	α_L (ft)	t_1 (y)	Q (cfs)
B.1.a	100	2.5	1.0
B.1.b	100	1.0	1.0
B.1.c	0.001	2.5	1.0
B.1.d	100	2.5	0.5

Table 6
Common parameters for subcases B.1.a, B.1.b, B.1.c, and B.1.d.

Parameter	Symbol	Value
Hydraulic conductivity	K	0.005 ft/s
Aquifer thickness	B	20.0 ft
Porosity	ϕ	0.30
Ratio of longitudinal to transverse dispersivity	α_L/α_T	1.0
Grid size in x direction	Δx	900 ft
Grid size in y direction	Δy	900 ft
Number of grid increments in x direction	N_x	9
Number of grid increments in y direction	N_y	[a]
Concentration of injected water	C_0	100.0%

[a] MOC requires an extra layer of grid cells outside a constant head boundary. For this reason, there are 11 grid cells in the MOC modeling, but only 9 in the FLOTRAN modeling.

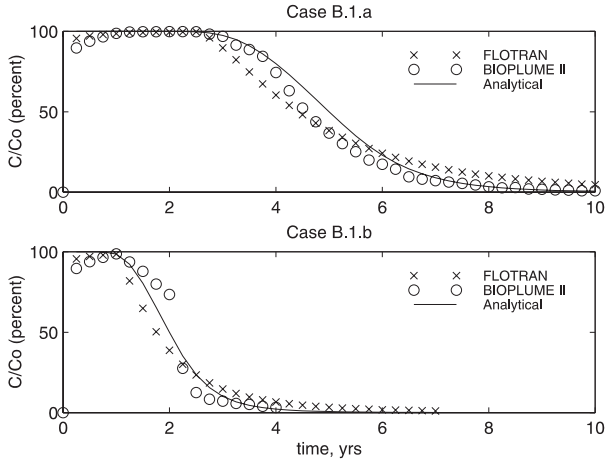

Fig. 9. Test B.1, concentration breakthrough curves in injection/extraction well – FLOTRAN vs. BIOPLUME II.

4.2.2. Test B.2: radial flow: injection well and extraction well

The second case tested by El-Kadi [10] was a recharge/recovery doublet. In this case, on a similar grid

Table 7
Simulation B.1, average absolute errors for FLOTRAN and BIOPLUME II for injection/extraction from a single well

Test	Compared to Gelhar/Collins	
	FLOTRAN (% of C_0)	BIOPLUME II (% of C_0)
B.1.a	6.6	3.4
B.1.b	5.0	6.6
B.1.c	12.9	6.9
B.1.d	7.4	6.7

there is an injection well 2700 ft (3 cells) from a recovery well pumping at the same flow rate. Javandel et al. [30] coded a semi-analytical solution to the purely advective transport in this situation. The model, called RESSQ, calculates the velocity field in a domain defined by injection and production wells, and tracks the contaminant front away from the injection well along a fixed number of streamlines emanating from the injection well. The concentration in the recovery well is determined by averaging contaminant concentrations among the streamlines entering the well. When the contaminant front reaches the recovery well along a given streamline the concentration at the well immediately jumps to its new value. The number of streamlines modeled determines the smoothness of the resulting breakthrough curve.

The recharge/recovery doublet was simulated on a 9×10 MOC grid, and therefore on a 9×8 FLOTRAN grid, since the extra layer of cells was not required (see Table 6, footnote). Fig. 10 shows the MOC setup for the simulation. The FLOTRAN setup is identical, with minor changes along the boundaries to account for the differences in boundary conditions between the two models. Other input parameters are the same as in Table 5, except that $Q_{in} = Q_{out} = 1.0$ cfs.

The resulting concentration breakthrough curves are shown in Fig. 11. Two features are evident from the first runs: (1) The solution given by FLOTRAN does not fluctuate like the MOC/BIOPLUME II solution does, and (2) the FLOTRAN concentrations are also about 3/4 of the RESSQ value.

In the 9×8 grid runs, neither model reached the concentrations predicted by RESSQ. The reason for this was that the model domain was simply too small. The contaminant was impinging on the constant head and no-flow boundaries. In order to more accurately model this scenario, the model domain was enlarged. Increasing the model domain to a 14×16 (or 14×18) grid and retaining the same grid size (900×900 ft^2) improved the results. In addition, a mesh refinement was performed with 225×225 ft^2 grid blocks. Runs were made with

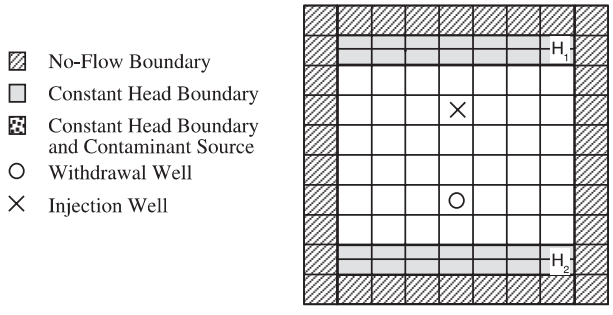

Fig. 10. Test B.2, aquifer model for the recharge/recovery doublet.

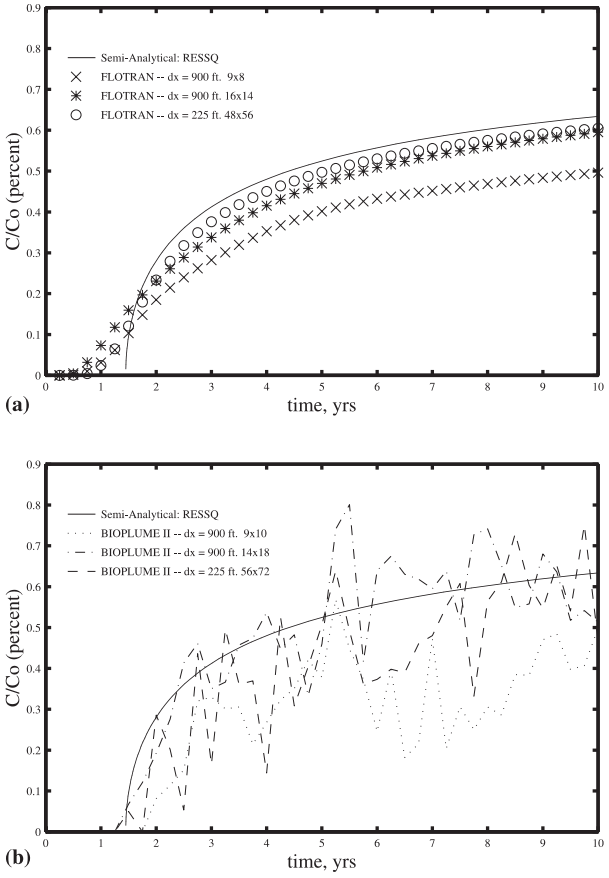

Fig. 11. Test B.2, concentration breakthrough curves at the recovery well for the recharge/recovery pair.

both FLOTRAN and BIOPLUME II using the refined grids. These results are also shown in Fig. 11.

Fig. 11a shows the resulting concentration breakthrough at the recovery well for the FLOTRAN simulations. A significant improvement (from 26.8% error at the breakthrough well to 12.2%) is observed by simply increasing the size of the model domain, and an additional improvement (to 10.7%), especially near the breakthrough time, is seen with the mesh refinement. A further mesh refinement (not shown) improves the results by about 0.1%. Errors for this simulation are given as percent differences from the RESSQ solution at the last time step.

Fig. 11b shows the results of the same simulations done with BIOPLUME II. In all three simulations, the concentration in the recovery well fluctuates. In the original simulation, the concentration fluctuates around a curve about 25% below the RESSQ solution, which is where the original FLOTRAN solution lies. Increasing the model domain improves the simulation in that the fluctuations are centered more closely on the RESSQ solution, however the amplitude of the fluctuations is not reduced. Mesh refinement does not improve the results. A similar run was performed with MT3D,

to determine if the observed behavior is typical of the Method of Characteristics; the behavior was very much like BIOPLUME II, and the results are not shown.

4.3. Tests vs. Bioplume II

The next test of FLOTRAN (Test C) is a direct comparison with BIOPLUME II in a case assuming instantaneous reaction of hydrocarbon with oxygen. The comparisons were performed by taking the same conceptual model for a hypothetical site and applying it to both models. The conceptual model involves an aquifer domain of $1100 \times 700 \times 10$ m^3, with a source of contamination 150 m from the upstream boundary. The initial oxygen concentration is 5000 μg/l, and oxygen enters the upstream boundary at a concentration of 5000 μg/l. The source was assumed to be active for 60 years. Other relevant model parameters are given in Table 8.

The hydrocarbon plume was created using a continuing source modeled by 3 wells side by side. Using the same input parameters for FLOTRAN and BIOPLUME II, a direct comparison of the models was possible. The results for hydrocarbon concentration along the centerline of the plume at several points in time are shown in Fig. 12. FLOTRAN and BIOPLUME II agree well in this simulation. Excluding the cells upstream of the wells, for which the agreement was rather poor, the average difference between the FLOTRAN and BIOPLUME II solutions agreed within 1.9%, averaged over all 40 time steps. Near the source, the hydrocarbon concentrations vary by up to 11%, due to oscillations in the BIOPLUME II simulation caused by particles moving from one cell to another, and discrete particle creation at the well. A mesh refinement was performed, halving the grid size in the direction of flow. BIOPLUME II still showed some oscillation near the source, and away from the source, the hydrocarbon concentrations were consistently lower than with FLOTRAN, and the mass balance errors in BIOPLUME II were on the order of 30–60%.

Table 8
Model parameters for FLOTRAN vs. BIOPLUME II Test

Model parameter	Value
Number of grid cells	25×15
Hydraulic conductivity	1×10^{-4} m/s
Porosity	0.3
Δx, Δy	50 m
Thickness	10 m
Dispersivity	30 m
Gradient	8×10^{-4} m/m
Injection rate	1×10^{-4} m^3/s (over 3 cells, 0.25, 0.5, 0.25)
Injection concentration	10,000 μg/l
Background O_2 concentration	5000 μg/l
Stoichiometric factor	3 mg_{O_2}/mg_{HC}

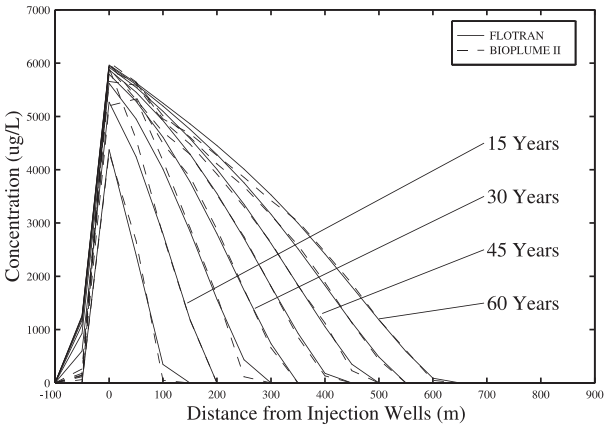

Fig. 12. Test C, FLOTRAN vs. BIOPLUME II comparison – concentration along the centerline of the plume for 10, 20, 30, 40, 50 and 60 yr of simulation.

4.4. Partially saturated flow and transport test

The final test case tests the ability of FLOTRAN to model flow and transport in a partially saturated media. We assumed a domain $[0,20] \times [0,20] \times [0,20]$ ft^3, with constant pressure head boundary conditions of 5 and 12 ft on the top ($z = 20$) and bottom ($z = 0$), respectively, and no-flow conditions on the sides. Initial pressure head was specified by $\Psi(x,y,z) = 12 - z$. The media was heterogeneous, with hydraulic conductivity of 0.57 ft/day everywhere except in the region $[1,15] \times [1,15] \times [10,15]$, where conductivity was set to 0.0057 ft/day. Inflow concentration of 5 mg/ft^3 was enforced for $5 < x < 9$, $10 < y < 14$ ft, at the top boundary. Elsewhere inflow concentration was assumed to be zero.

The functions θ and K are similar to functions used in a test case described in [3]. In particular,

$$\theta(\psi) = \left\{ \begin{array}{ll} \frac{\theta_s - \theta_r}{[1+(\alpha|\psi|)^n]^m} + \theta_r, & \psi < 0 \\ \theta_s, & \psi \geqslant 0 \end{array} \right\}$$

and

$$K(\psi) = \left\{ \begin{array}{ll} K_s \frac{\{1-(\alpha|\psi|^{(n-1)}[1+(\alpha|\psi|^n]^{-m}\}^2}{[1+(\alpha|\psi|)^n]^{m/2}}, & \psi < 0 \\ K_s, & \psi > 0 \end{array} \right\},$$

where $\theta_s = 0.368$, $\theta_r = 0.102$, $\alpha = 3.35$, $m = 0.5$ and $n = 2$. K_s is the saturated hydraulic conductivity. The specific storage was set to zero, and longitudinal and transverse dispersion coefficients of 0.1 and 0.01 ft were used, respectively.

The 3-D contaminant solution at time 10 days on a $40 \times 40 \times 40$ uniform mesh is given in Fig. 13. The deviation in the plume due to the low conductivity zone is

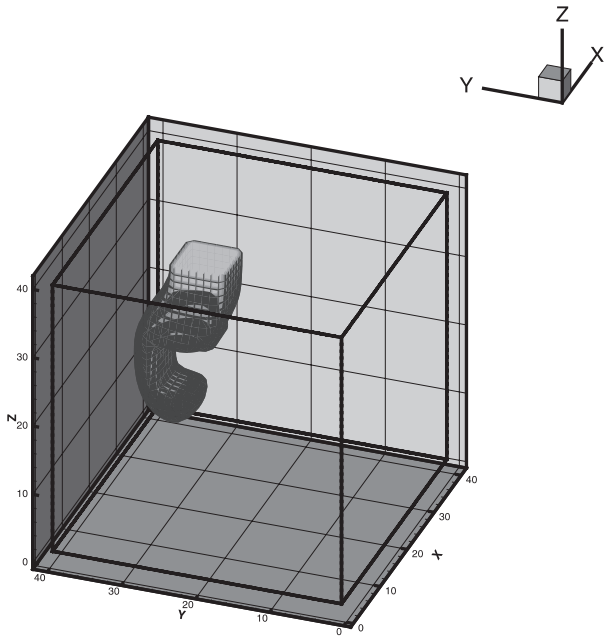

Fig. 13. Three-dimensional contaminant solution at $t = 10$ days on uniform $40 \times 40 \times 40$ mesh.

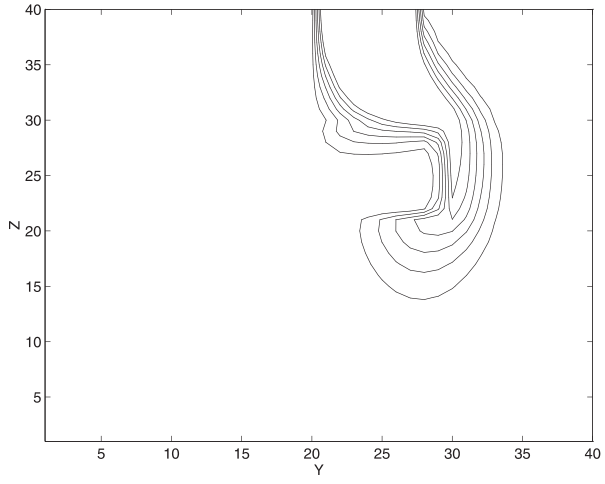

Fig. 14. Two-dimensional slice through contaminant solution along $x = 6.5$. Time = 10 days, $40 \times 40 \times 40$ uniform mesh.

apparent. A 2-D slice through the solution along the plane $x = 6.5$ is shown in Fig. 14. A comparison solution on a $20 \times 20 \times 20$ mesh is shown in Fig. 15. While the solutions are similar, the solution on the finer mesh is much better resolved. In Fig. 16, we show the solution computed on a $40 \times 40 \times 40$ non-uniform mesh, with refinement around the plume. This solution is slightly sharper than the uniform grid solution in Fig. 14. The contour levels in these plots are 0.5, 1, 1.5, 2, 2.5 and 3 mg/ft^3.

In these runs, the initial flow time step was set to around 0.05 days. The first few flow time steps required

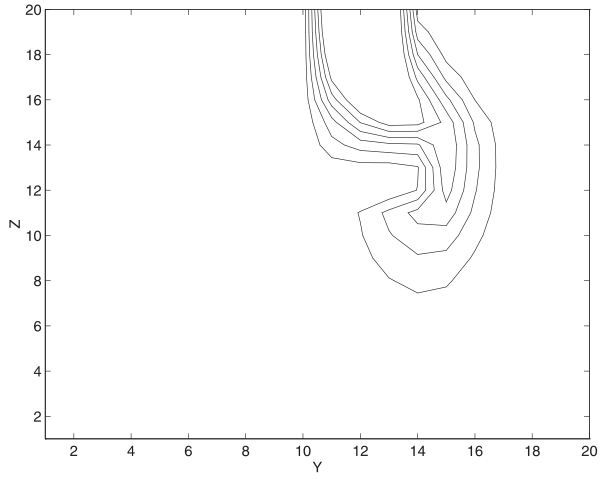

Fig. 15. Two-dimensional slice through contaminant solution along $x = 6.5$. Time = 10 days, $20 \times 20 \times 20$ uniform mesh.

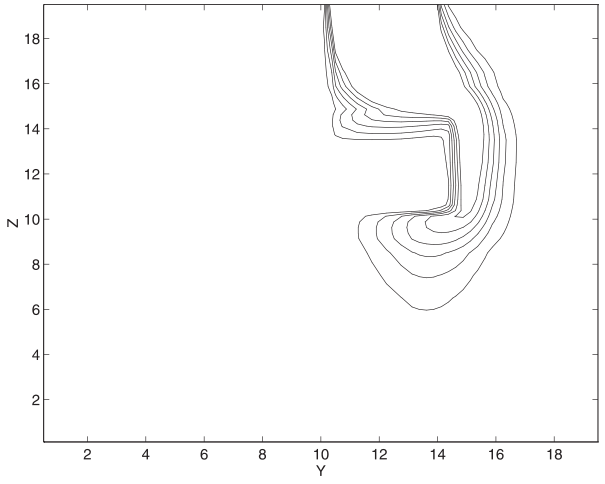

Fig. 16. Two-dimensional slice through contaminant solution along $x = 6.5$. Time = 10 days, $40 \times 40 \times 40$ nonuniform mesh.

around 10 Newton iterations to converge. After the initial infiltration, the number of Newton iterations decreased and the flow time step was increased until a steady state was reached.

5. Conclusions

FLOTRAN has been tested by comparing it to analytical, semi-analytical, and numerical solutions to the ground water flow and contaminant transport equations. In testing against analytical solutions, the code performed very well, matching the analytical solution almost exactly for the 1-D tests. In the 2-D test with a continuous source, a mesh refinement was performed, and the model performed well on the fine and medium

meshes, indicating that the cell Peclet number should be less than 3, and that near wells, the cell volume can affect observed concentrations due to mixing. In the 2-D test with a slug source, it matched the analytical solution well, especially at later times. At earlier times, the difference between a point source and a finite width source was evident in the solutions.

In the 3-D analytical test, FLOTRAN performed well, matching the shape and concentrations of the HPS solution very closely at a variety of locations. MT3D also performed well on this test, however FLOTRAN gave nearly identical results in about 1/10 of the computational time. The tests against analytical solutions show that the formulation of the approximations used in FLOTRAN is correct, and that the code does not add excessive numerical error to the solution. The tests re-emphasize the known fact that the mesh size can be an important factor in numerical simulations.

The semi-analytical testing of FLOTRAN was performed using modeling parameters designed to stress the numerical capabilities of a model. In these tests, under radial flow conditions with square cells, the model adds some numerical dispersivity to the solution. The authors have noted similar results in other non-uniform flow tests. In cases of uniform flow, as in Test A.1, it adds almost no numerical dispersivity. The code performed quite well on these tests, which indicates that it is robust enough to simulate non-ideal scenarios and still give results reasonably close to reality. In the same tests, BIOPLUME II produced a breakthrough curve that oscillated in concentration every time a particle passed over the boundary of the cell containing the well.

In testing FLOTRAN against BIOPLUME II in 2-D mode, the two models gave results that are similar in shape and magnitude. The FLOTRAN solution, however, is strictly monotonic, increasing steadily as the injectant pervades the aquifer. The BIOPLUME II solution fluctuates by over 10% as particles pass from cell to cell, taking all their mass with them. In addition, since the number of particles introduced at the well is not directly linked to the volume injected at the well, the BIOPLUME II solution loses mass, and can suffer from large mass balance errors.

FLOTRAN's modularity provides for extension of the model to incorporate alternate reaction scenarios. Holder et al. [14] have incorporated reaeration through the vadose zone using Fick's law into FLOTRAN. Their findings indicate that reaeration may be an important factor in modeling natural attenuation.

Overall, FLOTRAN has proved to be an efficient and accurate numerical model, which has performed well in a variety of tests. Its advantages include the use of advanced numerical techniques, and computational efficiency, which allows for more refined grids, improving model accuracy while not increasing model run times.

Acknowledgements

Although the research described in this article was supported through the National Science Foundation's Graduate Traineeship in Computational Environmental Science and Engineering Grant No. GER9355087 to Rice University, it has not been subjected to Agency Review and therefore does not necessarily reflect the reviews of the agency, and no official endorsement should be inferred. The third author was supported in part by National Science Foundation Grant DMS-9805491.

References

[1] Arbogast T, Wheeler MF, Yotov I. Mixed finite elements for elliptic problems with tensor coefficients as cell-centered finite differences. SIAM J. Numer. Anal. 1997;34:828–52.
[2] Bell JB, Dawson CN, Shubin GR. An unsplit higher order Godunov scheme for scalar conservation laws in two dimensions. J. Comput. Phys. 1988;74:1–24.
[3] Celia MA, Bouloutas ET, Zarba RL. A general mass conservative numerical solution for the unsaturated flow equation. Water Resour. Res. 1990;26:1483–96.
[4] Clement TP, Sun Y, Hooker BS, Petersen JN. Modeling natural attenuation of contaminants in saturated ground water. In: In situ and on-site Bioremediation. New Orleans, LA: Battelle Press, 1997:37–42.
[5] Dawson CN. Godunov-mixed methods for immiscible displacement. Int. J. Numer. Meth. Fluids 1990;11:835–47.
[6] Dawson CN. Godunov-mixed methods for advective flow problems in one space dimension. SIAM J. Numer. Anal. 1991;28:1282–309.
[7] Dawson CN. Godunov-mixed methods for advection–diffusion equations in multidimensions. SIAM J. Numer. Anal. 1993;30:1315–32.
[8] Dawson CN, Wheeler MF. Time-splitting methods for advection–diffusion-reaction equations arising in contaminant transport. ICIAM '91, Philadelphia, PA, Society for Industrial and Applied Mathematics: 1992:71–82.
[9] Dennis JEJ, Schnabel RB. Numerical methods for unconstrained optimization and nonlinear equations. Englewood Cliffs, NJ: Prentice-Hall, 1983.
[10] El-Kadi AI. Applying the USGS mass-transport model (MOC) to remedial actions by recovery wells. Ground Water 1988;26(3):281–8.
[11] Galya DP. A horizontal plane source model for ground-water transport. Ground Water 1987;25(6):733–9.
[12] Gelhar LW, Collins MA. General analysis of longitudinal dispersion in nonuniform flow. Water Resour. Res. 1971;7(4):1511–21.
[13] Holder AW. Testing and validation of FLOTRAN: a ground water flow and contaminant transport model. MS, Rice University: Houston, TX, 1995.
[14] Holder AW, Bedient PB, Hughes JB. Modeling the impact of oxygen reaeration on natural attenuation. Bioremediation J. 1999;3(2):137–49.

[15] Huyakorn PS, Kretschek AG, Broome RW, Mercer JW, Lester BH. Testing and validation of models for simulating solute transport in ground-water: Development, evaluation, and comparison of benchmark techniques. International Ground Water Modeling Center, Holcombe Research Institute, Butler University, Indianapolis, IN, 1984.
[16] Konikow LF, Bredehoeft JD. Computer model of two-dimensional solute transport and dispersion in ground water. Washington, DC, Automated Data Processing and Computations Techniques or Water Resources Investigations of the US Geological Society, 1978.
[17] McDonald MG, Harbaugh AW. A modular three-dimensional finite-difference ground-water flow model. Open File Report 83-875, US Department of the Interior, USGS National Center, Reston, Virginia, 1984.
[18] Ogata A, Banks RB. A solution of the differential equation of longitudinal dispersion in porous media. 411-A, 7p, USGS, 1961.
[19] Rifai HS, Bedient PB, Wilson JT, Miller KM, Armstrong JM. Biodegradation modeling at an aviation fuel spill site. J. Env. Eng. 1988;5:1007–29.
[20] Sauty JP. An analysis of hydrodispersive transfer in aquifers. Water Resour. Res. 1980;16(1):145–58.
[21] Valocchi AJ, Malmstead M. Accuracy of operator splitting for advection–dispersion-reaction problems. Water Resour. Res. 1992;28(5):1471–6.
[22] van der Heijde PKM, Huyakorn PS, Mercer JW. Testing and validation of ground water modeling. Practical Applications of Ground Water Modeling, Ohio State University, National Water Well Association: 1985:472.
[23] Warwick JJ, Stoffregen R. Impact of grid orientation in ground water contaminant transport modeling using the USGS MOC model. International Symposium on Ground Water in Practice, Nashville, TN, ASCE, 1991:7–12.
[24] Weiser A, Wheeler MF. On convergence of block-centered finite differences for elliptic problems. SIAM J. Numer. Anal. 1988;25:351–75.
[25] Wheeler MF, Dawson CN. An operator-splitting method for advection–diffusion-reaction problems. MAFELAP IV, London: Academic Press, 1988:463–482.
[26] Wilson JL, Miller PJ. Two-dimensional plume in uniform ground-water flow. Journal of the Hydraulics Division, ASCE 104 (HY4) 1978:503–514.
[27] Woodward C, Dawson CN. To appear in SIAM J. Numerical Analysis. Analysis of expanded mixed finite element methods for a nonlinear parabolic equation modeling flow into variably saturated porous media.
[28] Yeh GT, Ward DS. FEMWATER, a finite element model of water flow through saturated-unsaturated porous media. ORNL-5567, Oak Ridge National Laboratory, Oak Ridge, Tennessee, 1980.
[29] Zheng C. MT3D, a modular three-dimensional transport model user's manual. Rockville, MD: S.S. Papadopulos, 1991.
[30] Javandel et al., 1984.